RMetS
Royal Meteorological Society

Response of oceanic cyclogenesis metrics for NARGIS cyclone: a case study

Naresh Krishna Vissa,[1] A. N. V. Satyanarayana[1]* and B. Prasad Kumar[2]

[1]*Centre for Oceans, Rivers, Atmosphere and Land Sciences, Indian Institute of Technology, Kharagpur, West Bengal 721 302, India*
[2]*Department of Ocean Engineering and Naval Architecture, Indian Institute of Technology, Kharagpur, West Bengal 721 302, India*

*Correspondence to:
A. N. V. Satyanarayana, Centre for Oceans, Rivers, Atmosphere and Land Sciences, Indian Institute of Technology, Kharagpur, West Bengal 721 302, India.
E-mail:
anvsatya@coral.iitkgp.ernet.in*

Abstract

In this study, variability of two oceanic cyclogenesis metrics, tropical cyclone heat potential (TCHP) and effective oceanic layer for cyclogenesis (EOLC) in the Bay of Bengal (BoB) during NARGIS cyclone is investigated. EOLC represents the geopotential thickness of near surface stratified layer forms because of the spread of low salinity waters due to fresh water influx from rivers and precipitation. Climatological fields of TCHP and EOLC reveal that NARGIS translated towards the region of higher EOLC as seen in the observations. A maximum daily sea surface cooling of 2 °C is observed along the right and rear side of NARGIS track. Copyright © 2013 Royal Meteorological Society

Keywords: tropical cyclone heat potential; effective oceanic layer for cyclogenesis; sea surface cooling

1. Introduction

The first oceanic metric, which considers integration of sub-surface temperature up to isotherm corresponding to 26 °C water depth is called oceanic heat content (OHC) or tropical cyclone heat potential (TCHP) (e.g. Leipper and Volgenau, 1972; Sadhuram *et al.,* 2004; Price, 2009). TCHP exceeding 60 kJ cm^{-2} provide valuable information of the ocean thermal state beyond the initial sea surface temperature (SST) (Lin *et al.,* 2008). The limitations and applicability of TCHP over different oceanic basins are reviewed by several researchers (e.g. Goni and Trinanes, 2003; Sadhuram *et al.,* 2004; Price, 2009). Murty *et al.* (2000a, 2002, 2008) proposed another metric called effective oceanic layer for cyclogenesis (EOLC), which accounts for both temperature and salinity at near surface stratified layer and linearly related to outgoing long wave radiation (OLR). Higher EOLC regions are characterized with warmer temperatures, lower surface salinity; high heat potential and specific humidity in the surface air. EOLC is also helpful in determining near surface circulation in the regions influenced by low salinity waters (Gopalakrishna *et al.,* 2002). The surface stratified layer (∼0–30 m) decouples the thermocline processes and appears to guide the movement of weather disturbance.

In recent years, satellite and *in situ* observations have been widely utilized in understanding the upper ocean response to tropical cyclones (e.g. Goni and Trinanes, 2003; Subrahmanyam *et al.,* 2005; Mahapatra *et al.,* 2007; Vissa *et al.,* 2012a). Kikuchi *et al.* (2009) studied the initiation process of NARGIS using multi-satellite observations. On the basis of their study, it was seen that NARGIS initiated from unusual strong intra-seasonal westerly event allied with Madden-Julian oscillation (MJO) in the eastern Indian Ocean during middle of April. Kikuchi and Wang (2010) reported the role of tropical intra-seasonal oscillation in the formation of NARGIS on a climatological point of view. Yamada *et al.* (2010) address the role of sub-tropical jets assigning the reasons behind abnormal track, its intensification under characteristic environmental flow. McPhaden *et al.* (2009) studied the oceanic and atmospheric interactions for NARGIS, using *in situ* and satellite observations. Lin *et al.* (2009) reported warm anomalies in the surface and sub-surface layers mentioning on the critical issue of rapid intensification (defined as ≥30 kts intensification in 24 h) just before the landfall. Yu and McPhaden (2011) conducted a comprehensive data analysis, in order to understand the occurrence of SST front over the central Bay of Bengal (BoB) prior to the formation of NARGIS. Reale *et al.* (2009) emphasized the improvements in track forecast skill of NARGIS 4 days in advance. For this purpose, assimilated three-dimensional atmospheric data from atmospheric infrared sounder (AIRS) temperature retrievals was used. Numerical simulations were conducted using non-hydrostatic model as well as with ensemble prediction to reproduce the rapid intensification of NARGIS (e.g. Kuroda *et al.,* 2010; Saito *et al.,* 2010). The above-mentioned studies have not reported the role of EOLC as a metric to understand the translation of NARGIS. Keeping this in view, the objective of the present study is to understand the variability of cyclogenesis metrics (EOLC, TCHP) during different

epochs of NARGIS utilizing available *in situ*, satellite observations and comprehensive ocean atlas (COA) for Indian Ocean (Prasad Kumar *et al.,* 2009).

2. Data and methods

Temperature and salinity (T/S) profiles for this study were obtained from ten different Array for Real-time Geostrophic Oceanography (ARGO) floats during the period 17 April to 16 May 2008 (nearly ±10 day window of NARGIS passage) within the vicinity of its track. In addition, available RAMA buoy (90.0°E/15.0°N) daily T/S profile observations during the period 10 March 2008 to 30 April 2008 were used. Reynolds version 2 (RV2) (Reynolds *et al.,* 2007) high resolution ($0.25° \times 0.25°$) daily SST from 27 April to 3 May 2008 were taken. RV2 SST is the blended AVHRR and AMRS-E SST by optimum interpolation technique, this product also uses the *in situ* data from ships and buoys for the adjustment of satellite bias with respect to the *in situ* data. The monthly climatology during April to May was taken from high spatial resolution ($0.25° \times 0.25°$) COA developed for the Indian Ocean which utilizes ARGO data (e.g. Prasad Kumar *et al.,* 2009; Vissa *et al.,* 2012b). ARGO gridded data at 10 days interval with $1°$ spatial resolution generated from individual ARGO profiles using objective analysis method (Udaya Bhaskar *et al.,* 2007) during 2002–2009 for the month of April is utilized in this study. In addition to this, April month climatology of World Ocean Atlas 2009 (WOA09) having a spatial resolution of $1° \times 1°$ (Locarnini *et al.,* 2009; Antonov *et al.,* 2010) was used in this study. More details can be found in the NODC webpage (http://www.nodc.noaa.gov/OC5/WOA09/pr_woa09.html).

From the available *in situ* observations and ocean climatology, TCHP was computed using the following equation:

$$\text{TCHP} = \rho C_p \int_{Z_{26}}^{0} (\overline{T} - 26)\, dZ \qquad (1)$$

where ρ and C_p are the mean quantities of density (kg m^{-3}) and specific heat of sea water at constant pressure (J kg^{-1} C^{-1}) respectively from surface (first level of ARGO profile) to isotherm level corresponding to $26\,°C$ (Z_{26}). $\overline{T}$ is the mean temperature of the two consecutive layers.

The EOLC was computed from the mean specific volume anomaly (α) which mathematically can be expressed as:

$$\text{EOLC} = \int \alpha \cdot dp \qquad (2)$$

where '*dp*' is the pressure interval and the limits of integration extends from surface to 30 m. These limits of integration vary from ∼5 to 30 m depth for ARGO profiles.

2.1. Comparison of April month temperature and salinity (T/S) fields at 30 m level for BoB with COA, WOA09 and gridded ARGO data

COA is prepared for the Indian Ocean, which comprises temperature and salinity (T/S) fields at standard depths similar to the World Ocean Atlas (WOA), up to a maximum depth of 1000 m with a spatial resolution of quarter-degree. All available ARGO profiling floats during the period 2001–2006 was utilized in preparation of this comprehensive atlas. For the data-sparse regions past quality-checked ocean station data (OSD) and profiling float data (PFL) information was included along with the WOA. For more details about the COA, refer to the published work of Prasad Kumar *et al.* (2009). The T/S maps at 30 m level for the month of April from COA was compared with WOA09 and gridded ARGO data which is shown in Figure 1. Figure 1(a)–(c) represents the 30 m depth temperature for WOA09, COA and gridded ARGO respectively. Similarly salinity fields are shown in Figure 1(d)–(f) respectively. The justification behind considering the 30 m level for comparison of T/S fields are: (1) both the metrics TCHP and EOLC account for this level in computation and (2) influence of ARGO in COA can be seen in the near surface level. One can find the clear differences between the COA and WOA09 and close resemblance between the COA and gridded ARGO observational fields in both temperature and salinity. The differences between COA and WOA09 T/S fields are attributed because of the inclusion of ARGO and past OSD in the preparation of COA, which leads to its high spatial resolution, and the numerical algorithm used in the preparation of COA explained in the work of Prasad Kumar *et al.* (2009).

3. Results and discussion

The trajectory of NARGIS along with the locations of ARGO floats and RAMA buoy is shown in Figure 2. The ARGO floats are grouped as (a)–(j) based on float ID which have repetitive cycle of 4–10 days providing T/S profiles (Vissa *et al.,* 2012a). RV2 SST daily differences during 27 April to 2 May and a week difference (27 April to 3 May) for NARGIS are shown in Figure 3. RV2 SST difference from 30 April to 29 April (Figure 3(c)) was found to be maximum among all the daily differences which were about 2 °C along the west of 88°E. Over the central bay (88°E–92°E, 14°N–16°N) a cooling of about 1 °C was observed (Figure 3(d) and (e)) over this region NARGIS got intensified in the presence of low salinity waters (Yu and McPhaden, 2011). The daily sea surface cooling is noticed on the right and real side of the NARGIS track. Week RV2 SST difference of about 2–3 °C was noticed along the rear and right side of the NARGIS track. From the available ARGO profiling floats (a)–(j) the isothermal, isohaline and isopycnal layer depths (ITLD, IHLD and IPLD, respectively) were estimated. Mixed layer depth (MLD) is defined
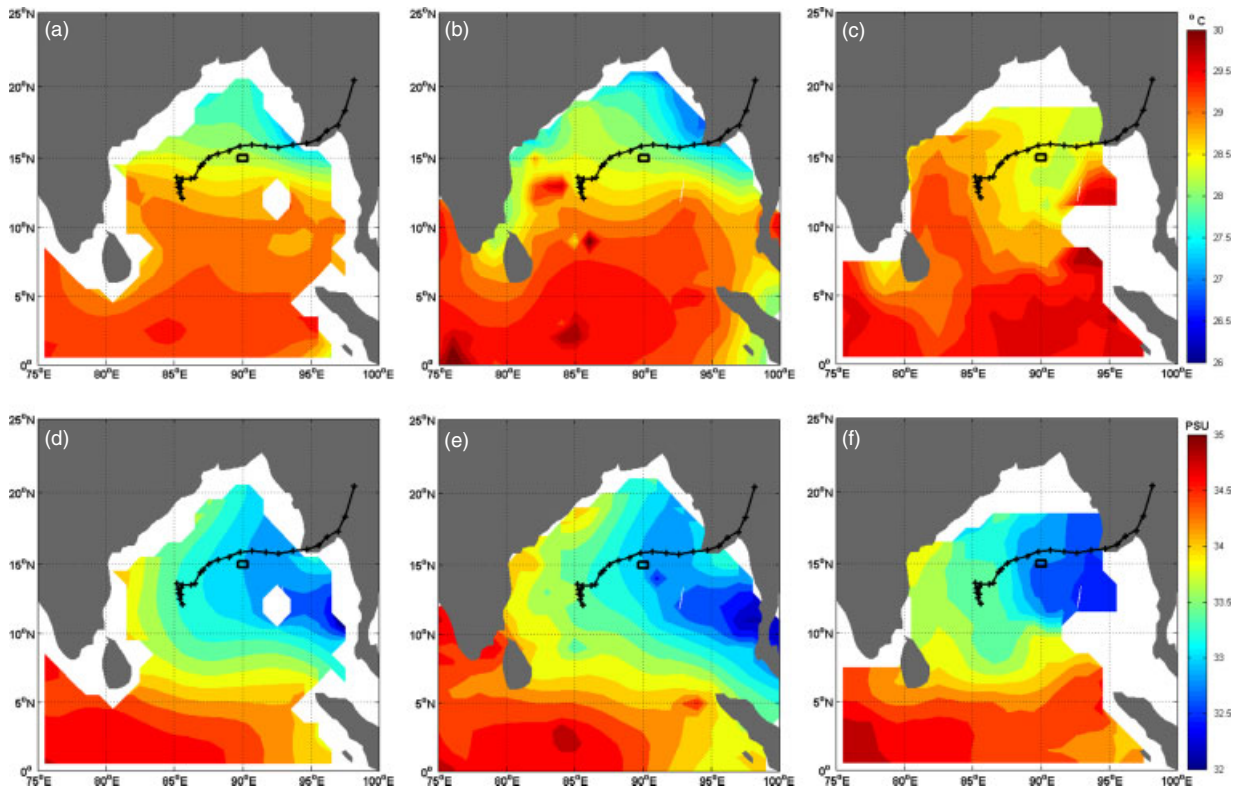
Figure 1. Distribution of temperature (top panel) and salinity (bottom panel) at 30 m level in the month of April from (a,d) WOA09, (b,e) COA and (c,f) gridded Argo data. NARGIS track and location of the RAMA buoy (rectangle) are overlaid.
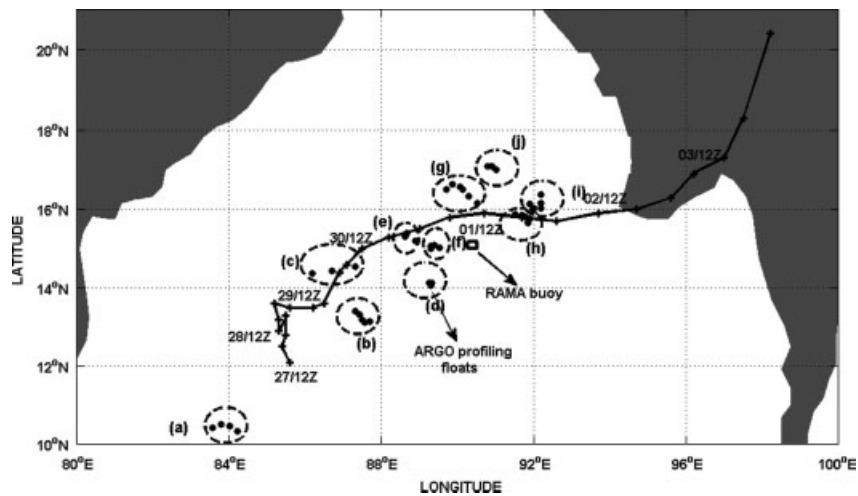

Figure 2. Track of the NARGIS cyclone and the corresponding position of the ARGO floats (circles), RAMA Buoy (rectangle) and the groping of ARGO floats ((a–j), dotted circles).

as the shallowest of the ITLD, IHLD or IPLD. Barrier layer thickness (BLT) is defined as the difference between the ITLD and IPLD (Helber *et al.*, 2012). MLD and BLT for ARGO profiling floats (a)–(j) are given in the Table I. Prior to the NARGIS passage absence or thin BL (~10 m) was noticed from all profiling floats. After the NARGIS passage over two locations (d, h floats as shown in Figure 2) formation of BL was seen after the NARGIS passage could be attributed because of the intense precipitation.

During the same period Yu and McPhaden (2011) also reported the absence of barrier layer from RAMA

buoy (15°N/ 90°E) observations. Observed features are consistent with the pre-monsoon barrier layer climatological fields of BoB (Thadathil *et al.*, 2007; Vissa *et al.*, 2012b). The absence of barrier layer supports strong turbulent mixing Wang *et al.* (2011) and further leads to sea surface cooling. Sea surface cooling of 2 °C occurred in the region where cyclone translation speed (speed of the cyclone, U_H) was relatively low (4 m s^{-1}), whereas cooling of 1 °C was observed over the region with high U_H (about 8 m s^{-1}). The changes in steering flow (steering flow represents the average of zonal mean winds
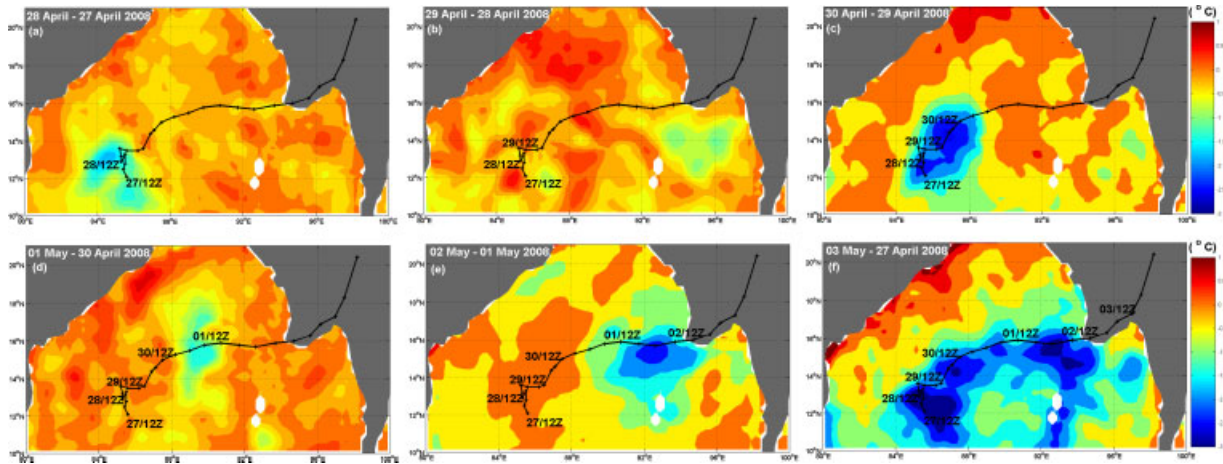
Figure 3. Daily RV2 SST differences from 27 April–2 May (a–f) and week RV2 SST difference (3 May–27 April) over laid by NARGIS cyclone track with corresponding dates.
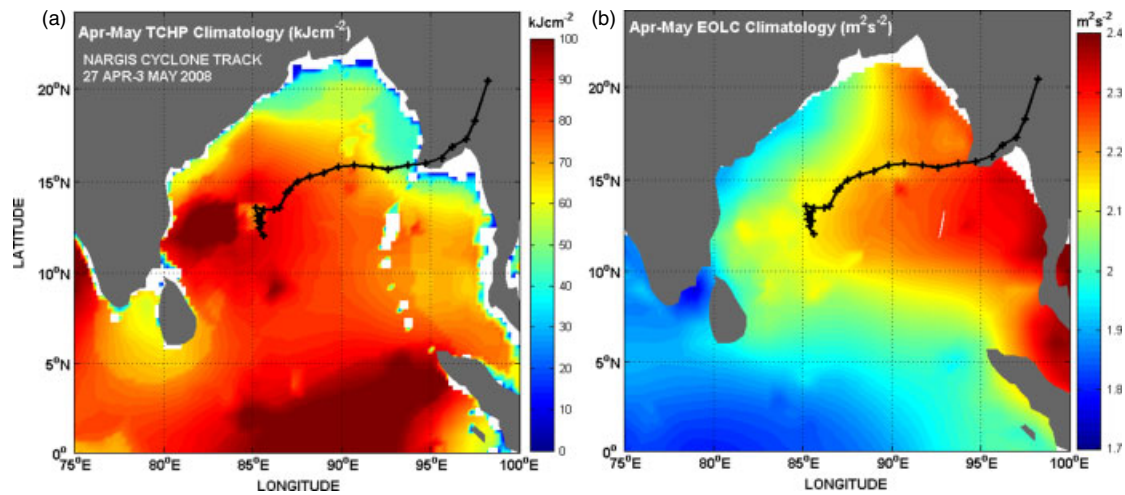

Figure 4. Climatological fields of TCHP (a), EOLC (b) during pre-monsoon season.

between 700 and 300 hPa) from 1.5 to 5.5 m s^{-1} after the re-curvature is responsible for NARGIS acceleration (Yamada *et al.,* 2010). The rightward SST bias for the NARGIS cyclone can be examined in the following ways. Price (1981) and Gierach and Subrahmanyam (2008) suggested that rapidly moving cyclones are having the rightward SST bias. As the cyclone progresses, the wind stress veers clockwise direction at a fixed point along the right side of the cyclone track. In the Northern Hemisphere, Coriolis force acts on the ocean currents in the same direction of the wind stress on the right side of the cyclone track. Because of the transfer of energy from the cyclone and to the ocean currents, it leads to the rightward bias of the intense inertial currents. In turn rightward bias of the near inertial currents in the wake of the cyclone leads the stronger entrainment on the right side of the track, favouring the rightward bias of the SST cooling (Price, 1981; Jiang *et al.,* 2009). Surface winds of the NARGIS possessed a strong right asymmetry winds (Ueno and Bessho, 2011). Deo *et al.* (2004) suggested that during cyclone passage ocean response is strong in the case of right asymmetric winds than that of

left asymmetric winds in the Northern Indian Ocean. Stronger right asymmetry winds, high U_H during rapid intensification period and stronger entrainment on the right hand side of the track which is also evident from the absence of BL are responsible for the rightward SST bias for the NARGIS cyclone.

Cyclone-induced upwelling is dependent on the speed of the storm and it is negligible for the fast moving storms. Upwelling contributes a greater role and enhancement of the SST cooling (Price, 1981). Numerical and observational studies by Price (1981), Bender *et al.* (1993) and Rao *et al.* (2007) suggest that sea surface cooling is inversely related to speed of the storm, i.e. fast, medium and slow moving storms results in a low, medium and high SST cooling, which also holds good for this study. These observations are supported by the works of Rao *et al.* (2010), Dare and McBride (2011). Passage of a cyclone results in sea surface cooling and further leads to decrease of surface heat flux and TCHP. TCHP would be a suitable metric in demonstrating the ocean thermal field for the cyclone-induced cooling due to air sea heat exchanges (Price, 2009).

Table I. Variation of mixed layer depth (MLD) and barrier layer thickness (BLT) from the selected ARGO floats during NARGIS period. The locations of (a)–(j) are shown in Figure 2.

ARGOID	Date	Latitude (°N)	Longitude (°E)	MLD (m)	BLT (m)
2900885 (a)[a]	170408	83.58	10.41	9.0	0
	220408	83.79	10.51	14.5	0
	270408	84.02	10.46	19.4	0
4900673 (b)[a]	230408	87.43	13.33	9.5	0
	280408	87.5	13.2	39.5	0
	20508	87.57	13.13	9.2	0
	80508	87.69	13.16	9.3	0
2900107 (c)[a]	140508	86.19	14.38	25.7	0
	240408	87.31	14.55	10.6	4.9
	40508	86.71	14.43	10.3	5.4
4900672 (d)[a]	280408	89.29	14.07	29.5	0
	30508	89.31	14.14	29.5	9.8
	80508	89.25	14.14	29.5	19.8
2900755 (e)[a]	210408	88.64	15.31	9.4	0
	10508	88.67	15.4	9.3	0
	110508	88.89	15.21	9.6	0
4900671 (f)[a]	230408	89.3	15.02	9.4	10.3
	280408	89.32	15.06	19.7	0
	30508	89.39	15.09	19.2	10
	80508	89.52	15.03	9.3	0
4900675 (g)[a]	230408	91.69	15.85	9.3	0
	280408	91.79	15.82	9.5	0
	30508	91.9	15.77	29.7	0
	80508	91.86	15.66	9.7	0
2901074 (h)[a]	260408	89.87	16.64	14.3	0
	10508	90.06	16.57	34.6	9.5
	60508	90.13	16.51	34.4	9.8
	110508	90.29	16.34	14.4	4.8
2901075 (i)[a]	260408	92	16.02	9.3	0
	60508	92.19	16.02	9.3	0
	110508	92.18	16.16	13.9	0
2900756 (j)[a]	210408	90.8	17.09	9.1	0
	10508	90.91	17.1	19.5	0
	110508	91.01	17	9.5	0

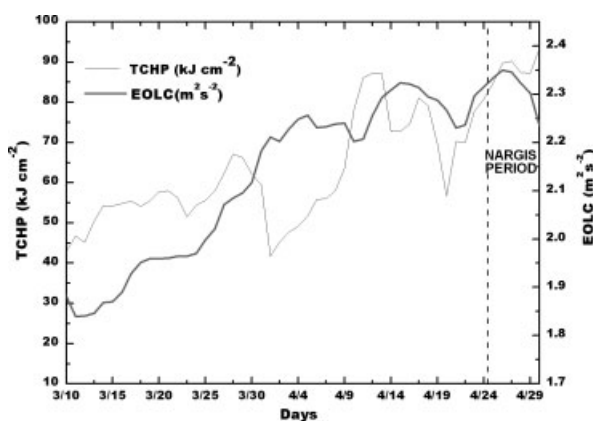**Figure 5.** Daily variability of TCHP, EOLC from RAMA buoy (15°N/90°E).

The climatological fields of TCHP and EOLC based on COA during April to May are shown in Figure 4. The maximum value of TCHP about 100 kJ cm^{-2} is noticed in the south-western and central bay. At the re-curvature location ($\sim$85.0°E/13.5°N) of NARGIS the computed TCHP was about 60 kJ cm^{-2}. At the same location McPhaden *et al.* (2009) reported relatively higher values of TCHP (order of about 80–90 kJ cm^{-2}) which may be due to coarse resolution of WOA used in their study. The variation of EOLC (Figure 4) is in contrast with that of TCHP. High values of EOLC (>2.2 m^2 s^{-2}) and lower values of TCHP (between 50–60 kJ cm^{-2}) are noticed for NARGIS.

The variations in TCHP along the western and eastern BoB are characterized with the anticyclonic gyre (ACG) and cyclonic gyre (CG) (Murty *et al.*, 2000b, Sadhuram *et al.*, 2004). Central BoB is characterized with higher SST and salinity, and north-eastern BoB and northern Andaman Sea are characterized with lower SST and salinity (Murty *et al.*, 2000a. This could be responsible for the spatial variability of the EOLC in the western and eastern BoB.

Lin *et al.* (2009) reported higher SSTs during NARGIS and the same is attributed to the presence of the low salinity waters maintaining warmer temperatures. Yu and McPhaden (2011) reported the existence of strong SST front in BoB before the NARGIS passage which is coupled with high sea surface height anomalies (SSHA). This is attributed to downwelling Rossby waves and convergence of fresh water. The physical mechanisms stated above are responsible for higher EOLC during the NARGIS period. The atmospheric components such as the equivalent potential temperature of 350 K (Yamada *et al.*, 2010), higher surface relative humidity and vertically integrated water vapour flux (Li *et al.*, 2012) observed during the NARGIS passage also in turn attributed towards higher EOLC. The work of Lin *et al.* (2009) reported rapid intensification of NARGIS prior to landfall. This matches with higher EOLC reported in this study.

The day to day variations of TCHP and EOLC utilizing the available RAMA buoy (90.0°E/15.0°N) observations during the period from March 10 to April 30 are shown in Figure 5 over which NARGIS had passed. An overall increasing trend was noticed in both TCHP and EOLC during the approach of NARGIS towards RAMA buoy location. The period from 28 March to 1 April (Figure 5) shows a drop in TCHP along with an increasing trend in EOLC. During this period, reduction of 1 °C in SST along with higher wind speeds (15 m s^{-1} on 28 March reducing to 6 m s^{-1} on 01 April) from QuikSCAT records was noticed. The total accumulated rainfall vary from 30 mm (29 March) to 1 mm (1 April) as seen from TRMM 3B42 records associated with sharp decrease in short wave radiation flux of 150 W m^{-2} (29 March). The drop in TCHP was seen almost for 3 days (Figure 5). The steady rise in EOLC during this period can be attributed because of freshwater influx from heavy rainfall. From 1 April onwards TCHP regain its increasing trend until 20 April with a marginal reduction during 14 April. On 20 April, a marginal drop in EOLC and substantial reduction in TCHP were seen. Interestingly, during this period weak wind along with no rainfall exist. The reason behind this abnormal reduction in TCHP is inconsistent with prevailing weather conditions.
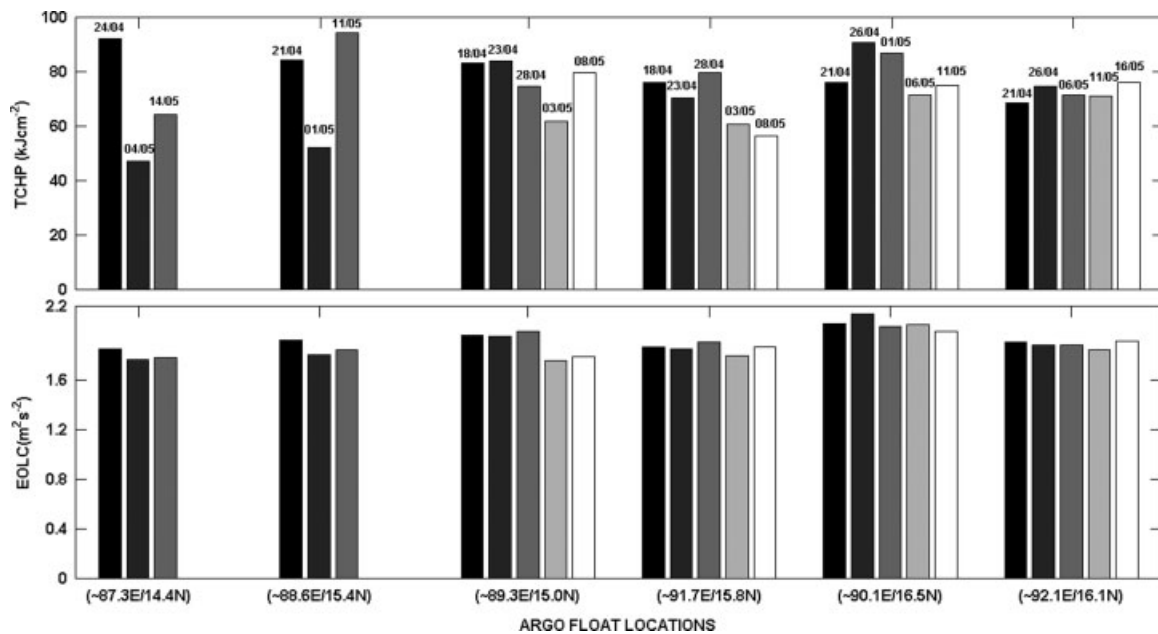
Figure 6. TCHP and EOLC variations derived from ARGO floats during different epochs of NARGIS over central BoB.

TCHP and EOLC computed from ARGO floats (grouping shown in circles) during different epochs of NARGIS are presented in Figure 6. A decrease in TCHP is noticed over rear side of NARGIS track (during slow translation speed) associated with sea surface cooling. This can be attributed to air-sea heat exchange as reported by Price (2009). In contrast, for higher translation speed along with rapid intensification of NARGIS, higher TCHP and EOLC are noticed. During the slow moving period, separation of rain bands and decreased precipitable water content was observed from satellite infrared and microwave imageries, whereas after the re-curvature during the fast moving period a recovery of the axisymmetric rain bands near the centre was reported (Yamada *et al*., 2010). Interestingly, over the lower EOLC region, rain bands are separated whereas in the higher EOLC region recovery of rain bands structure and rapid intensification occurred for NARGIS cyclone. The coincidence of higher EOLC and increased U_H was observed during the rapid intensification of NARGIS event. NARGIS is translated from lower EOLC ($\sim$1.85 m^2 s^{-2}) regions to higher EOLC ($\sim$2.15 m^2 s^{-2}) regions (Figure 6). This is because of the strong zonal salinity gradient in the April 2008 as reported by (Yu and McPhaden, 2011). On the basis of these results it could be established that significant variations seen in TCHP is unable to correlate well with the forward motion and intensification of NARGIS. Unlike TCHP, the variations in EOLC demonstrate a better consistency with storm motion and its intensification.

4. Summary

The study demonstrates that forward motion of NARGIS is towards the region of higher EOLC as seen

from climatological maps and *in situ* observations. After the passage of NARGIS cyclone different cooling regions are noticed, i.e. moderate cooling over the lower EOLC regions and low cooling over the higher EOLC regions, which is also concurrent with the translation speed of the cyclone. Although TCHP is widely used as a metric to identify the possible cyclogenesis location, this study advocates the importance of EOLC as another metric which can be used as an indicator to predict forward motion of the storm.

References

Antonov JI, Seidov D, Boyer TP, Locarnini RA, Mishonov AV, Garcia HE, Baranova OK, Zweng MM, Johnson DR. 2010. In *World Ocean Atlas 2009. Vol. 2, Salinity, NOAA Atlas NESDIS*, Levitus S (ed), Vol. **69**. NOAA: Silver Spring, MD; 184.

Bender MA, Ginis I, Kurihara Y. 1993. Numerical simulations of tropical cyclone-ocean interaction with a high-resolution coupled model. *Journal of Geophysical Research* **98**(D12): 23245–23263, DOI: 10.1029/93JD02370.

Dare RA, McBride JL. 2011. Sea surface temperature response to tropical cyclones. *Monthly Weather Review* **139**: 3798–3808, DOI: 10.1175/MWR-D-10-05019.1.

Deo AA, Gane DW, Salvekar PS. 2004. Behaviour of the upper ocean in response to an idealized symmetric and asymmetric Indian Ocean cyclone in opposite hemisphere. *Journal of Indian Geophysical Union* **8**(3): 211–222.

Gierach MM, Subrahmanyam B. 2008. Biophysical responses of the upper ocean to major Gulf of Mexico hurricanes in 2005. *Journal of Geophysical Research* **113**: C04029, DOI: 10.1029/2007JC004419.

Goni GJ, Trinanes JA. 2003. Ocean thermal structure monitoring could aid in the intensity forecast of tropical cyclones. *Eos Transactions, Americal Geophysical Union* **84**(51), DOI: 10.1029/2003EO510001.

Gopalakrishna VV, Murty VSN, Sengupta D, Shenoi SSC, Araligidad N. 2002. Upper ocean stratification and circulation in the northern Bay of Bengal during southwest monsoon of 1991. *Continental Shelf Research* **22**: 791–802.

Helber RW, Kara AB, Richman JG, Carnes MR, Barron CN, Hurlburt HE, Boyer T. 2012. Temperature versus salinity gradients below the ocean mixed layer. *Journal of Geophysical Research* **117**: C05006, DOI: 10.1029/2011JC007382.

Jiang X, Zhong Z, Jiang J. 2009. Upper ocean response of the South China Sea to Typhoon Krovanh (2003). *Dynamics of Atmospheres and Oceans* **47**: 165–175.

Kikuchi K, Wang B. 2010. Formation of tropical cyclones in the northern Indian Ocean associated with two types of tropical intraseasonal oscillation modes. *Journal of the Meteorological Society Japan* **88**: 475–496.

Kikuchi K, Wang B, Fudeyasu H. 2009. Genesis of tropical cyclone Nargis revealed by multiple satellite observations. *Geophysical Research Letters* **36**: L06811, DOI: 10.1029/2009GL037296.

Kuroda T, Saito K, Kunii M, Kohno N. 2010. Numerical simulation of Myanmar cyclone Nargis Part I: forecast experiment with NHM and simulation of storm surge. *Journal of the Meteorological Society Japan* **88**: 521–545.

Leipper D, Volgenau D. 1972. Upper ocean heat content of the Gulf of Mexico. *Journal of Physical Oceanography* **2**: 218–224.

Li W-W, Wang C, Wang D, Yang L, Deng Y. 2012. Modulation of low-latitude west wind on abnormal track and intensity of tropical cyclone Nargis (2008) in the Bay of Bengal. *Advances in Atmospheric Sciences* **29**(2): 407–421.

Lin I-I, Wu C-C, Pun I-F, Ko D-S. 2008. Upper ocean thermal structure and the western North Pacific category-5 typhoons. Part I: Ocean features and category-5 typhoon's intensification. *Monthly Weather Review* **136**: 3288–3306.

Lin I-I, Chen C-H, Pun I-F, Liu W-T, Wu C-C. 2009. Warm ocean anomaly, air sea fluxes, and the rapid intensification of tropical cyclone Nargis (2008). *Geophysical Research Letters* **36**: L03817, DOI: 10.1029/ 2008GL035815.

Locarnini RA, Mishonov AV, Antonov JI, Boyer TP, Garcia HE, Baranova OK, Zweng MM, Johnson DR. 2009. In *World Ocean Atlas 2009. Vol. 1, Temperature, NOAA Atlas NESDIS*, Levitus S (ed), Vol. **68**. NOAA: Silver Spring, MD; 184.

Mahapatra DK, Rao AD, Babu SV, Srinivas C. 2007. Influence of coast line on upper ocean's response to the tropical cyclone. *Geophysical Research Letters* **34**: L17603, DOI: 10.1029/2007GL030410.

McPhaden MJ, Foltz GR, Lee T, Murty VSN, Ravichandran M, Vecchi GA, Vialard J, Wiggert JD, Yu L. 2009. Ocean–atmosphere interactions during cyclone Nargis. *Eos Transactions, Americal Geophysical Union* **90**(7), DOI: 10.1029/2009EO070001.

Murty VSN, Sarma MSS, Tilvi V. 2000a. Seasonal cyclogenesis and the role of near-surface stratified layer in the Bay of Bengal. Proceedings of PORSEC (A-092), NIO, Goa, India, 5–8 December, 2000.

Murty VSN, Gupta GVM, Sarma VV, Rao BP, Jyothi D, Shastri PNM, Supraveena Y. 2000b. Effect of vertical stability and circulation on the depth of the chlorophyll maximum in the Bay of Bengal during May–June 1996. *Deep Sea Research Part I* **47**: 859–873.

Murty VSN, Subrahmanyam B, Sarma MSS, Tilvi V, Ramesh Babu V. 2002. Estimation of sea surface salinity in the Bay of Bengal using outgoing longwave radiation. *Geophysical Research Letters* **29**(16): 1775, DOI: 10.1029/2001GL014424.

Murty VSN, Sarma MSS, Jenson GV, Vidya PJ. 2008. Impact of freshwater influx on the cyclogenesis, tracks of cyclones and air-sea coupling over the Bay of Bengal. Proceedings volume of Workshop on Natural Hazards and Coastal Processes of Indian Coast (NHACPIC-2008), 30 April 2008, 54–63 http://drs.nio.org/drs/handle/2264/1081 [accessed 28 March 2012].

Prasad Kumar B, Barman R, Dube SK, Pandey PC, Ravichandran M, Nayak S. 2009. Development of a new comprehensive ocean atlas for Indian Ocean utilizing ARGO data. *International Journal of Climatology* **30**: 185–196.

Price JF. 1981. Upper ocean response to a hurricane. *Journal of Physical Oceanography* **11**: 153–175.

Price JF. 2009. Metrics of hurricane-ocean interaction: vertically-integrated or vertically-averaged ocean temperature? *Ocean Science Discussions* **6**: 909.

Rao AD, Sujata D, Babu SV, Indu J. 2007. Numerical modeling of cyclone impact on the ocean- a case study of the Orissa Supper cyclone. *Journal of Coastal Research* **23**(5): 1245–1250.

Rao AD, Madhu J, Jain I, Ravichandran M. 2010. Response of subsurface waters in the eastern Arabian Sea to tropical cyclones. *Estuarine, Coastal and Shelf Science* **89**: 267–276.

Reale O, Lau WK, Susskind J, Brin E, Liu E, Riishojgaard LP, Fuentes M, Rosenberg R. 2009. AIRS impact on the analysis and forecast track of tropical cyclone Nargis in a global data assimilation and forecasting system. *Geophysical Research Letters* **36**: L06812, DOI: 10.1029/2008GL037122.

Reynolds RW, Smith TM, Liu C, Chelton DB, Casey KS, Schlax MG. 2007. Daily high-resolution blended analyses for sea surface temperature. *Journal of Climate* **20**: 5473–5496.

Sadhuram Y, Rao BP, Rao DP, Shastri PNM, Subrahmanyam MV. 2004. Seasonal variability of cyclone heat potential in the Bay of Bengal. *Natural Hazards* **32**: 191–209.

Saito K, Kuroda T, Kunii M, Kohno N. 2010. Numerical simulation of Myanmar cyclone Nargis Part 2: ensemble prediction. *Journal of the Meteorological Society Japan* **88**: 547–570.

Subrahmanyam B, Murty VSN, Sharp RJ, O'Brien JJ. 2005. Air-sea coupling during the tropical cyclones in the Indian ocean: a case study using satellite observations. *Pure and Applied Geophysics* **162**: 1643–1672.

Thadathil P, Muraleedharan PM, Rao RR, Somayajulu YK, Reddy GV, Revichandran C. 2007. Observed seasonal variability of barrier layer in the Bay of Bengal. *Journal of Geophysical Research* **112**: C02009, 18 PP, DOI: 10.1029/2006JC003651.

Udaya Bhaskar TVS, Ravichandran M, Devender R. 2007. An operational objective analysis system at INCOIS for generation of Argo Value Added Products. Report No. INCOIS-MOG-ARGO-TR-04-2007, Indian National Centre for Ocean Information Services, Hyderabad, Andhra Pradesh, India.

Ueno M, Bessho K. 2011. A statistical analysis of near-core surface wind asymmetries in typhoons obtained from QuikSCAT data. *Journal of the Meteorological Society Japan* **89**: 225–241, DOI: 10.2151/jmsj.2011-304.

Vissa NK, Satyanarayana ANV, Prasad KB. 2012a. Response of upper ocean during passage of MALA cyclone utilizing ARGO data. *International Journal of Applied Earth Observation and Geoinformation* **14**: 149–159.

Vissa NK, Satyanarayana ANV, Prasad Kumar B. 2012b. Comparison of Mixed Layer Depth and Barrier Layer Thickness for the Indian Ocean using two different Climatologies. *International Journal of Climatology* (conditionally accepted).

Wang X, Han G, Qi Y, Li W. 2011. Impact of barrier layer on typhoon-induced sea surface cooling. *Dynamics of Atmospheres and Oceans* **52**: 367–385.

Yamada H, Moteki Q, Yoshizaki M. 2010. The unusual track and rapid intensification of cyclone Nargis in 2008 under a characteristic environmental flow over the Bay of Bengal. *Journal of the Meteorological Society Japan* **88**(3): 437–453.

Yu L, McPhaden MJ. 2011. Ocean pre-conditioning of cyclone Nargis in the Bay of Bengal: interaction between Rossby waves, surface fresh waters, and sea surface temperatures. *Journal of Physical Oceanography* **41**: 1741–1755.